HAWC2 and BeamDyn: Comparison Between Beam Structural Models for Aero-Servo-Elastic Frameworks

Preprint

Christian Pavese and Taeseong Kim
DTU Wind Energy

Qi Wang, Jason Jonkman, and Michael A. Sprague
National Renewable Energy Laboratory

Presented at the European Wind Energy Association Annual Conference and Exhibition 2015 (EWEA 2015)
Paris, France
November 17–20, 2015

NREL is a national laboratory of the U.S. Department of Energy
Office of Energy Efficiency & Renewable Energy
Operated by the Alliance for Sustainable Energy, LLC

This report is available at no cost from the National Renewable Energy Laboratory (NREL) at www.nrel.gov/publications.

Conference Paper
NREL/CP-5000-65115
August 2016

Contract No. DE-AC36-08GO28308

NOTICE

This report is available at no cost from the National Renewable Energy Laboratory (NREL) at www.nrel.gov/publications.

Available electronically at SciTech Connect http:/www.osti.gov/scitech

Available for a processing fee to U.S. Department of Energy and its contractors, in paper, from:

U.S. Department of Energy
Office of Scientific and Technical Information
P.O. Box 62
Oak Ridge, TN 37831-0062
OSTI http://www.osti.gov
Phone: 865.576.8401
Fax: 865.576.5728
Email: reports@osti.gov

Available for sale to the public, in paper, from:

U.S. Department of Commerce
National Technical Information Service
5301 Shawnee Road
Alexandria, VA 22312
NTIS http://www.ntis.gov
Phone: 800.553.6847 or 703.605.6000
Fax: 703.605.6900
Email: orders@ntis.gov

Cover Photos by Dennis Schroeder: (left to right) NREL 26173, NREL 18302, NREL 19758, NREL 29642, NREL 19795.

NREL prints on paper that contains recycled content.

HAWC2 and BeamDyn: Comparison Between Beam Structural Models for Aero-Servo-Elastic Frameworks

Christian Pavese[1], Qi Wang[2], Taeseong Kim[1], Jason Jonkman[2], and Michael A. Sprague[2]

[1]DTU Wind Energy, DK-4000, Roskilde, Denmark
[2]National Renewable Energy Laboratory, Golden, CO 80401

cpav@dtu.dk

Abstract

This work presents a comparison of two beam codes for aero-servo-elastic frameworks: a new structural model for the aeroelastic code HAWC2 and a new nonlinear beam model, BeamDyn, for the aeroelastic modularization framework FAST v8. The main goal is to establish the suitability of the two approaches to model the structural behaviour of modern wind turbine blades in operation. Through a series of benchmarking structural cases of increasing complexity, the capability of the two codes to simulate highly nonlinear effects is investigated and analyzed. Results show that even though the geometrically exact beam theory can better model effects such as very large deflections, rotations, and structural couplings, an approach based on a multi-body formulation assembled through linear elements is capable of computing accurate solutions for typical nonlinear beam theory benchmarking cases.

1 Introduction

Wind turbine blades are highly complex composite structures, and their design presents advanced challenges. In recent years, the development of multimegawatt wind turbines has brought blade designers to explore different cost-effective solutions, including manufacturing larger, lighter, and more flexible wind turbine blades. The increase in size and flexibility in relation to the reduction in mass has augmented the importance of nonlinear effects related to the structural behaviour of the blades. These effects include large deflections and rotations along with structural couplings, such as bending-to-torsion. Hence, wind energy research started to focus on the necessity of developing models and tools able to accurately capture the response of these highly complex structures under aerodynamic loading.
In this paper, two beam models for aero-servo-elastic frameworks are presented, analyzed, and compared:

- A new linear anisotropic beam element implemented into the nonlinear aeroelastic multi-body code HAWC2 [1], developed by the Technical University of Denmark (DTU)
- A new nonlinear beam finite element (FE) model that uses the geometrically exact beam theory (GEBT), and for which spatial discretization is accomplished with Legendre spectral finite elements (LSFEs); the beam model is implemented as a module called BeamDyn [2][3] within the aeroelastic modularization framework FAST v8 [4], developed by the National Wind Technology Center at the National Renewable Energy Laboratory (NREL).

It is important to remark that even though the new HAWC2 beam element is based on a linear formulation, its implementation in a multibody system makes it possible to capture nonlinear effects, such as large rotations and translations. Hence, even if the structure in HAWC2 is modeled using several linear bodies, a comparison to the beam FE model implemented in BeamDyn can still be made even though the latter is based on a nonlinear formulation. Moreover, both of these structural codes have been separately verified and validated against results found in the literature and experimental data.

The purpose of this paper is not only to compare the accuracy of the two codes, but also to highlight the differences between the two approaches by setting up a specific series of benchmarking cases of increasing complexity. These cases involve only cantilever beams and an isolated wind turbine blade, whereas a full aeroelastic comparison will be presented in future works by the authors.

2 Approach

Highly flexible composite structures, such as wind turbine blades, can undergo large deflections without exceeding their specified elastic limit. Due to the geometry of their deformation, the behaviour of such structures is nonlinear and the solution becomes very complex. For this reason, and to face the complexity of these deformations, BeamDyn uses GEBT [5][6]. Exhaustive details related to the theory behind BeamDyn and its implementation in the FAST v8 state-space formulation are provided by [2][3]. This approach grants very high accuracy in solving highly nonlinear structural problems, but it has a high computational cost. To address the computation cost, BeamDyn has been implemented with LSFEs, which characteristically have exponential convergence rates for smooth solutions, as opposed to low-order FEs that have algebraic convergence (requiring fewer nodes for the same accuracy). HAWC2 uses a different method to face nonlinear effects due to large deflections, large rotations, and structural couplings. As reported in the introduction, the beam model of HAWC2 is based on a multi-body formulation assembled with linear anisotropic Timoshenko beam elements. A detailed description of this type of element is provided by [1]. The accuracy of this approach is, in general, lower than that of the GEBT. The advantages, with respect to a nonlinear beam model, are the much lower computational cost required to model a nonlinear problem and the possibility of augmenting the accuracy by increasing the number of bodies.
These two methods are compared using a series of benchmarking cases. The main purpose is to evaluate the accuracy of the two structural codes against highly nonlinear problems. It is important to remark that the first four cases investigated in this work are "extreme." The deflections and rotations computed for these nonlinear problems are not comparable to those typical of operating wind turbine blades. Nonetheless, the two structural codes have been used to simulate these limit cases to prove the suitability of both approaches to provide valid solutions related to the behaviour of twisted and curved structures and composite beams with complex layups.
The cases are listed below:

- Case 1: Static analysis of a cantilever beam under five constant bending moments applied at its free end
- Case 2: Static analysis of an initially twisted and an initially curved beam
- Case 3: Static analysis of a composite beam with a force applied at the free end
- Case 4: Dynamic analysis of a composite beam with a sinusoidal force applied at the free end
- Case 5: DTU 10-MW reference wind turbine (RWT) [8] blade natural frequencies.

The analysis of the performances and responses of the two beam models start from a simple and very common case (static bending of a cantilever beam) and move to a complex tailored wind turbine blade. Except for the DTU 10-MW RWT blade natural frequencies, the cases were already used to verify BeamDyn and are presented by [2][3]. Nonetheless, these cases were selected as the basis for this study, because they are suited to demonstrate the capabilities of the two codes to model structures that show nonlinear responses due to geometric and material couplings. The results obtained from the two codes were compared to results found in the literature or high-fidelity models generated using commercial, three-dimensional (3D), FE software such as ANSYS, Patran-Marc and Dymore.

3 Results

In this section, results for the each of the benchmarking cases are reported and discussed. Discrepancies between the two structural codes are highlighted and analyzed. The section is divided into five parts, one for each of the cases computed. Except for the last part of the study, which reports results concerning a wind turbine blade, very large displacements

and composite beams with complex layups are taken into account.

3.1 Case 1: Static analysis of a cantilever beam under five constant bending moments applied at its free end

Case 1 concerns the static deflection of a cantilever beam that is subjected at its free end to a constant negative moment around the x_2 axis. A system schematic is shown in Figure 1.

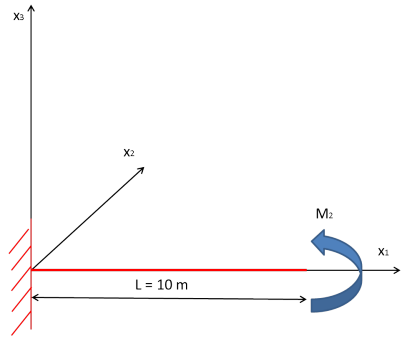

Figure 1: Description of the beam and the coordinate system for Case 1.

The length of the beam is 10 m and the input cross-sectional stiffness matrix is defined in Equation 1. In this paper, the stiffness matrices are presented in the coordinate system adopted by [9].

$$K = 10^3 \begin{bmatrix} 1770 & 0 & 0 & 0 & 0 & 0 \\ 0 & 1770 & 0 & 0 & 0 & 0 \\ 0 & 0 & 1770 & 0 & 0 & 0 \\ 0 & 0 & 0 & 8.16 & 0 & 0 \\ 0 & 0 & 0 & 0 & 86.9 & 0 \\ 0 & 0 & 0 & 0 & 0 & 215 \end{bmatrix} \quad (1)$$

where the units associated with the stiffness values are $K_{i,j}$ (N) and $K_{i+3,j+3}$ (N m^2) for $i,j = 1,2,3$. Further details on the data used are fully provided by [2]. The BeamDyn model is composed of two 5th- order LSFEs, whereas HAWC2 models uses 30 and 50 bodies, respectively. The negative moment applied around the x_2 axis is defined in Equation 2.

$$M_2 = \lambda \pi \frac{EI_2}{L} \quad (2)$$

where λ is a parameter used to scale M_2, from 0 to 2; E is the Young modulus; I_2 is the moment of inertia with respect to the axis x_2, and L is the total length of the beam. Table 1 shows the tip displacements computed by BeamDyn and HAWC2 compared to the analytical solution. The solution, reported in Equation 3, can be found in [10].

$$\begin{aligned} u_1(x_1) &= \rho \sin\left(\frac{l(x_1)}{\rho}\right) - l(x_1) \\ u_3(x_1) &= \rho \cos\left(1 - \frac{l(x_1)}{\rho}\right) \end{aligned} \quad (3)$$

where $\rho = \frac{EI_2}{M_2}$ and u_1 and u_3 are the displacements along the x_1 and x_3 axes, respectively, calculated at each node $l(x_1)$.

Table 1: Comparison of the beam tip displacements for all the applied bending moments.

λ	Sol. (u_3)	BD	H2-30b	H2-50b
0.4	-2.432 m	0.0%	0.5%	0.2%
0.8	-7.661 m	0.0%	1.3%	0.5%
1.2	-11.56 m	0.0%	1.2%	0.4%
1.6	-11.89 m	0.0%	1.3%	0.5%
2.0	-10.00 m	0.0%	5.1%	2.0%
λ	Sol. (u_1)	BD	H2-30b	H2-50b
0.4	5.50 m	0.0%	0.1%	0.0%
0.8	7.20 m	0.0%	0.3%	0.1%
1.2	4.80 m	0.0%	4.5%	1.7%
1.6	1.37 m	0.0%	22.7%	9.7%
2.0	0.00 m	0.00	-0.008 m	-0.01 m

In Table 1, *Sol.* indicates the analytical solution, *BD* the beam model BeamDyn, and *H2-30b* and *H2-50b* the HAWC2 structural model assembled with 30 and 50 bodies, respectively. For $\lambda = 2$, because the analytical solution of u_1 is 0.0, the results are reported in absolute values instead of percentages.
Figure 2 provides a visual representation of the beam displacement in longitudinal, x_3, and axial directions, x_1.
As the moment applied to the free end increases, the geometrically nonlinear effects of the benchmark problem become relevant. The tip displacement computed by BeamDyn is indistinguishable from the analytical solution; two 5th-order LSFEs is more than enough to achieve high accuracy and fewer nodes/elements is likely possible. Due to the use of linear elements, the structural model of HAWC2 is not fully able to catch this highly nonlinear behaviour. The increase in the number of bodies in HAWC2 to model the beam

reduces the error and improves the accuracy of the computed displacements.

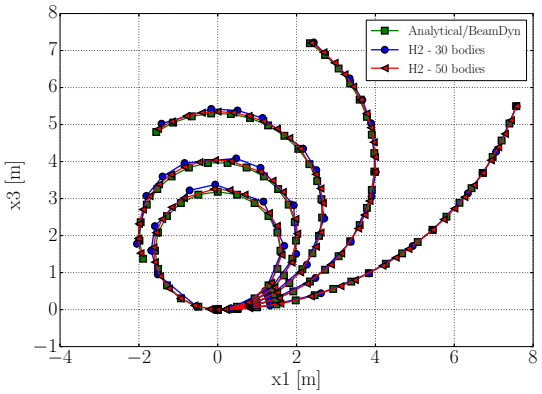

Figure 2: Bending of the cantilever beam in the x_1-x_3 plane. Five growing negative bending moments around the x_2-axis are applied at the free end on the beam. Circles: HAWC2 beam model with 30 bodies. Triangles: HAWC2 beam model with 50 bodies.

3.2 Case 2: Static analysis of an initially twisted and an initially curved beam

Beams characterized by initial twists and curvatures are analyzed for Case 2. First, a straight beam with an initial twist is considered (Figure 3). The beam is linearly twisted in the positive θ_1 direction from 0 degrees at the root to 90 degrees at the tip. Table 2 shows the material properties for A36 steel, the beam geometry, and the force applied at the free end along the negative x_3 axis. As in Case 1, the beam in BeamDyn is meshed with two 5th-order LSFEs, and the HAWC2 beam model is meshed with 30 bodies.

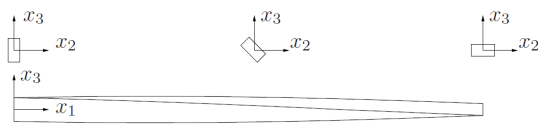

Figure 3: Representation of the twisted beam and the coordinate system for Case 2.

Table 2: Material properties (A36 steel), geometry (rectangular section), and tip force applied on the beam.

Property	Value
Elastic Modulus	200 GPa
Shear Modulus	79.3 GPa
Height	0.5 m
Width	0.25 m
Length	10 m
Force	4000 kN

The full description of the beam is also provided by [3]. The results for the twisted beam are shown in Table 3 and compared to the baseline results obtained from an extremely refined 3D ANSYS SOLID186 elements model.

Table 3: Comparison of the twisted beam tip displacements: ANSYS SOLID186 Model, BeamDyn, and HAWC2.

	u_1 [m]	u_2 [m]	u_3 [m]
ANSYS	-1.134	-1.714	-3.584
BeamDyn	0.13%	0.04%	0.15%
HAWC2	2.42%	1.92%	1.05%

The second part of Case 2 involves an initially curved beam. The benchmark problem for precurved beams was proposed by Bathe in 1979 [11]. Figure 4 shows the configuration of the curved cantilever beam. The beam lies in the plane defined by the positive x_1 direction and the negative x_2 direction. A force of 600 N is applied in the positive x_3 direction. The beam is defined by the 45-degree arc with 100-m radius centered at 100 m in the negative x_2 direction. The beam has a square cross-section geometry. As in Case 1, the cross-sectional stiffness matrix of the beam, computed using the geometry and the material properties provided by [11], is diagonal. The computed displacements for the static analysis are reported in Table 4 and a comparison to the results published by [11] is provided.

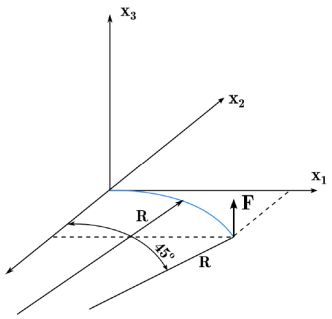

Figure 4: A sketch of the initially curved beam and the coordinate system for the second part of Case 2.

Table 4: Comparison of the curved beam tip displacements: Ref.[11], BeamDyn, and HAWC2.

	u_1 [m]	u_2 [m]	u_3 [m]
Bathe-Bolourchi [11]	-23.7	-13.4	53.4
BeamDyn	0.8%	0.8%	0.0%
HAWC2	2.1%	3.1%	0.0%

The tendency of the results computed by the two structural codes is the same for both the pre-twisted beam problem and the pre-curved benchmark cases. With the discretization applied, BeamDyn is able to better represent the nonlinear behaviour of twisted and curved beams (differences below 1%). HAWC2 computes tip displacements that are between 2% and 3% away from the solutions. Even though HAWC2 uses linear beam elements, the multibody approach is able to provide sufficiently accurate solutions for the large displacements considered in these two geometrically nonlinear problems.

3.3 Case 3: Static analysis of a composite beam with a force applied at the free end

The purpose of Case 3 is to compare the capability of HAWC2 to BeamDyn to simulate the behaviour of composite beams with an elastic coupling. A 10-m long cantilever composite box beam is considered. The coordinate system is the same as Case 1 (see Figure 1). BeamDyn and HAWC2 use the same meshes described for Case 2 (BeamDyn: two 5th-order LSFEs; HAWC2: 30 bodies). The cross-sectional stiffness matrix is shown in Equation 4.

$$K = 10^3 \begin{bmatrix} 1368.17 & 0 & 0 & 0 & 0 & 0 \\ 0 & 88.56 & 0 & 0 & 0 & 0 \\ 0 & 0 & 38.78 & 0 & 0 & 0 \\ 0 & 0 & 0 & 16.96 & 17.61 & -0.351 \\ 0 & 0 & 0 & 17.61 & 59.12 & -0.370 \\ 0 & 0 & 0 & -0.351 & -0.370 & 141.47 \end{bmatrix} \tag{4}$$

where the units associated with the stiffness values are $K_{i,j}$ (N), $K_{i,j+3}$ (N m) and $K_{i+3,j+3}$ (N m^2) for $i, j = 1, 2, 3$. A concentrated dead force of 150 N is applied in the positive direction of x_3 at the free tip of the beam. The displacements and rotations along the beam axis are plotted in Figure 5 and Figure 6, respectively. Due to the properties of the composite materials, coupling effects exist between the twist and the two bending modes (see Equation 4). For this reason, a consistent rotation around the x_1 axis can be observed in Figure 6.

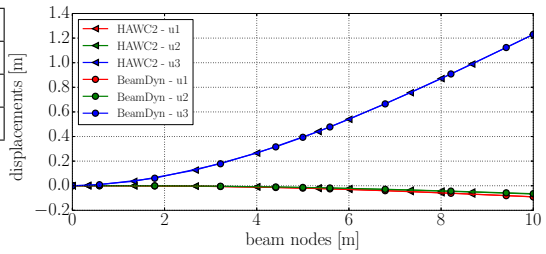

Figure 5: Displacements of the composite beam with respect to the nodal positions. Red: beam displacement of the nodes along the u_1 axis. Green: beam displacement of the nodes along the u_2 axis. Blue: beam displacement of the nodes along the u_3 axis. Triangles: HAWC2. Circles: BeamDyn.

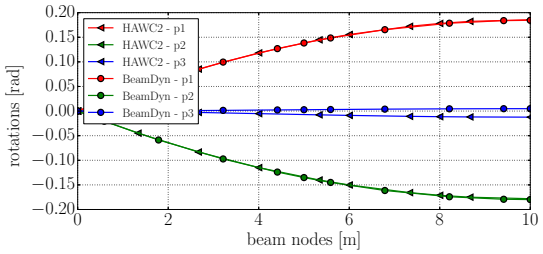

Figure 6: Rotations of the composite beam with respect to the nodal positions. Red: beam rotation of the nodes around the u_1 axis. Green: beam rotation of the nodes around the u_2 axis. Blue: beam rotation of the nodes around the u_3 axis. Triangles: HAWC2. Circles: BeamDyn.

The tip displacements and rotations are compared to Dymore [12], a finite-element-based multi-body dynamics code. Results are shown in Table 5.

Table 5: Comparison of tip displacements and rotations for Case 3.

	u_1 [m]	u_2 [m]	u_3 [m]
Dymore	-0.09064	-0.06484	1.22998
BeamDyn	0.0%	0.0%	0.0%
HAWC2	1.1%	3.7%	0.0%
	p_1 [rad]	p_2 [rad]	p_3 [rad]
Dymore	0.18445	-0.17985	0.00488
BeamDyn	0.0%	0.0%	0.0%
HAWC2	0.6%	1.0%	-153.1%

In Table 5, p_1, p_2, and p_3 indicates the rotation of the free-end node of the beam around the axis x_1, x_2, and x_3 respectively. BeamDyn is able to perfectly match the displacements and rotations computed by Dymore. The tip deflections computed by the structural beam model of HAWC2 are in good agreement with Dymore. The rotation around the x_3 axis shows a large discrepancy between HAWC2 and BeamDyn. This rotation is extremely small, and the one computed by HAWC2 is different in magnitude and sign from those computed by Dymore and BeamDyn. This difference can be better observed in Figure 6 (blue curves). The reason for this inconsistency lies in the formulation of the beam elements used by the two codes. Further numerical validations and eventual comparisons to experimental data are required to establish whether HAWC2 is able to accurately compute small rotations introduced by a structural coupling.

3.4 Case 4: Composite beam with a sinusoidal force applied at the free end

The objective of Case 4 is to compare HAWC2 and BeamDyn to composite beams under dynamic loading. The cantilever beam used is the same as that described in Case 3 as are the meshes used for the beam models. The coordinate system is the same as that used in Case 1 and shown in Figure 1. The cross-sectional mass matrix is presented in Equation 5.

$$M = 10^{-2} \begin{bmatrix} 8.538 & 0 & 0 & 0 & 0 & 0 \\ 0 & 8.538 & 0 & 0 & 0 & 0 \\ 0 & 0 & 8.538 & 0 & 0 & 0 \\ 0 & 0 & 0 & 1.4433 & 0 & 0 \\ 0 & 0 & 0 & 0 & 0.40972 & 0 \\ 0 & 0 & 0 & 0 & 0 & 1.0336 \end{bmatrix} \tag{5}$$

The units associated with the mass matrix values are $M_{i,i}$ (kg s^2 m^{-2}) and $M_{i+3,i+3}$ (kg s^2) for $i = 1, 2, 3$. A sinusoidal point dead force is applied in the x_3 direction. The force is described by Equation 6.

$$F_3(t) = A_F \sin \omega_F t \tag{6}$$

where the signal amplitude $A_F = 100\ N$ and the frequency $\omega_F = 10\ rad\ s^{-1}$. The displacements and rotations along the beam axis are plotted in Figure 7. Root forces and moments are plotted in Figure 8.

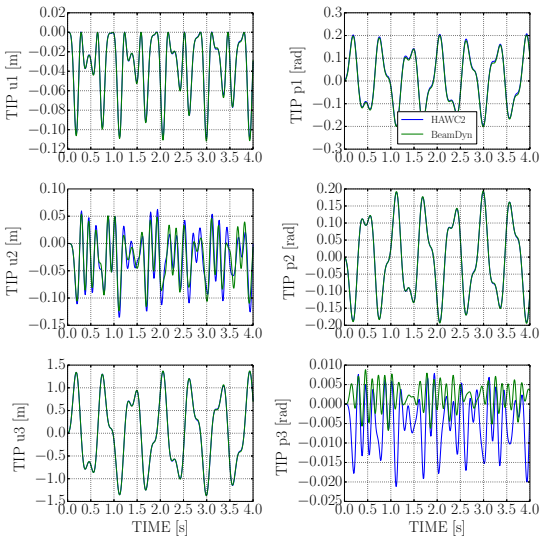

Figure 7: Tip displacements (left side, u_1, u_2, and u_3 from top to bottom) and rotations (right side, p_1, p_2, and p_3 from top to bottom) for 4-second simulations.

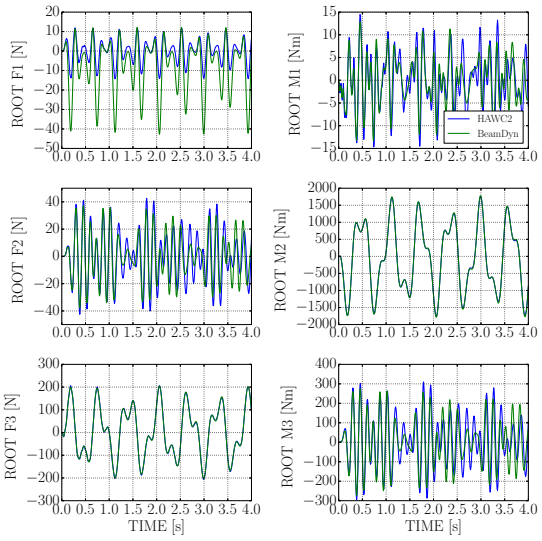

Figure 8: Root forces (left side, F_1, F_2, and F_3 from top to bottom) and moments (right side, M_1, M_2, and M_3 from top to bottom) for 4-second simulations.

On this dynamic benchmark case, BeamDyn and HAWC2 show good agreement, particularly in relation to the dynamics of the tip displacement and rotation in the direction where the force is applied. As happened for Case 3, the most consistent differences are registered for the rotation around the x_3 direction. This discrepancy is also the reason for the differences reported for the axial force F_1 (see Figure 8). The forces are projected on a fixed coordinate system placed at the root of the beam. BeamDyn and HAWC2 compute different rotations around the x_3 direction, and this has an impact on the component of the force projected on the x_1 axis. No other relevant discrepancies are registered between the forces and moments computed by HAWC2 and those computed by BeamDyn (see Figure 8).

3.5 Case 5: DTU 10-MW RWT blade natural frequencies

For the last case, the natural frequencies of the isolated DTU 10-MW RWT blade [8] are compared. In HAWC2, the natural frequencies of the blade are obtained directly from its eigenvalue solver. The beam is assembled with 26 bodies. The version of BeamDyn used for the current work was not developed with an eigenvalue solver. Therefore, two impulse forces of 4 kN are applied on the blade tip in the edgewise and flapwise directions. Power spectral densities (PSDs) are then computed from the tip displacement time series. The beam is meshed assembling 13 2nd-order elements. For this case study, more elements than the previous cases were used to better represent the complexity of such a tailored structure. The results obtained from HAWC2 and BeamDyn are compared to the natural frequencies computed with a Patran-Marc 3D FE model (20-noded layered continuum elements).
Figure 9 shows the PSDs of the two BeamDyn impulse test cases. Table 6 identifies the natural frequencies using the Patran model compared to those computed by BeamDyn and HAWC2.

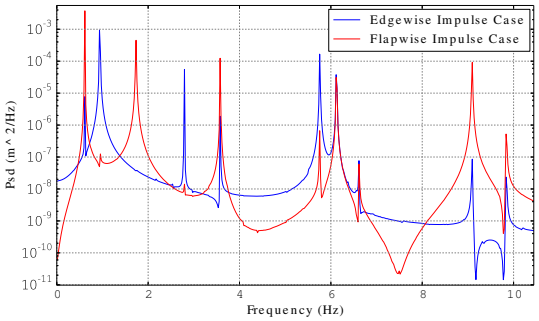

Figure 9: BeamDyn PSD of tip displacement in flapwise and edgewise directions for impulse load case. Blue curve: Flapwise tip displacement for an impulse force applied on the tip in the flapwise direction. Red curve: Edgewise tip displacement for an impulse force applied on the tip in the edgewise direction.

Table 6: Comparison of the DTU 10-MW RWT natural frequencies.

	FEM [Hz]	H2 [%]	BD [%]
1st Flap	0.615	-0.6%	0.0%
1st Edge	0.971	-4.2%	-3.8%
2nd Flap	1.764	-1.4%	-1.7%
2nd Edge	2.857	-3.7%	-2.2%
3rd Flap	3.592	-0.4%	-0.5%
1st Torsion	5.753	-1.7%	-0.1%
4th Flap	6.124	-1.1%	-0.1%
3rd Edge	6.151	-0.3%	-0.2%

The results show good agreement between HAWC2 and BeamDyn. The differences be-

tween the natural frequencies of the beam models from the full 3D FE model are in the same range. The largest discrepancy is registered for the first edgewise mode, with an approximate 4% difference between the beam models and the FE model. This discrepancy is because of the strategy used to model the trailing edge in the FE model, in which the 20-noded layered continuum elements allowed for a higher degree of tailoring compared to the input data provided in [8]. Consequently, this FE-modeling strategy resulted in a stiffer blade in the edgewise direction.

4 Conclusions

This paper presented comparison between two new structural codes for aero-servo-elastic frameworks: one developed by DTU Wind Energy and implemented in the nonlinear aero-servo-elastic multi-body code HAWC2, and the other, a nonlinear beam FE based on GEBT and called BeamDyn, developed by the National Wind Technology Center at NREL as a module for the modular framework FAST v8. These new beam models were implemented with the purpose of better representing the complex structural behaviour of modern wind turbine composite blades. To analyze the capabilities of the two codes, ad hoc benchmarking cases were selected. To test the limit ability of the two beam models to simulate nonlinear structural behaviours, four extreme case studies, called Case 1 to Case 4, were chosen, along with a final modal analysis involving a wind turbine blade, called Case 5. The results obtained from the two codes were compared to analytical results or high-fidelity models generated using commercial 3D FE software such as Dymore, ANSYS and Patran-Marc.
Case 1 considered static bending of a cantilever beam under five constant bending moments applied at its free end. Case 2 investigated initially twisted and initially curved beam with a force applied at the free end along the x3 axis direction. Both cases showed good agreement between HAWC2 and BeamDyn. In general, BeamDyn proved to have a greater capability to simulate extremely large displacements of beams subject to geometrical nonlinearities. HAWC2 demonstrated with sufficient accuracy its capability to model the first and second case, with the additional benefit of being able to increase the number of bodies for a more accurate solution without excessively compromising the computational cost. In Case 3 and Case 4, a composite beam with elastic coupling under static and dynamic loading, respectively, were analyzed. BeamDyn and HAWC2 were again in good agreement, except for a very small rotation generated by the structural coupling of the composite box cross-section. Because BeamDyn perfectly matched the target displacements and rotations provided for these two cases, further investigations are required to establish whether HAWC2 is able to model small rotations due to structural couplings. Last, the isolated DTU 10-MW RWT blade case showed the capability of both models to accurately compute the natural frequencies of a complex structure such as a wind turbine composite blade.
Given the results generated by both codes to simulate highly nonlinear structural problems, both approaches are considered suitable to properly model the complex behaviour of a wind turbine blade in operation.
Future work will provide an extensive comparison between the computational costs of the two structural codes. Full aeroelastic simulations will be taken into account, to provide a full overview regarding the capabilities of the two structural codes and the benefits that can be achieved with a full integration in aero-servo-elastic frameworks.

References

[1] Kim, T., Hansen, A. M. and Branner, K., *Development of an anisotropic beam finite element for composite wind turbine blades in multi-body system*, Journal of Renewable Energy, 2013, 59(2013) 172-183.

[2] Wang, Q., Sprague, M. A., Jonkman, J. and Johnson, N. *Nonlinear Legendre Spectral Finite Elements for Wind Turbine Blade Dynamics*, 32nd ASME Wind Energy Symposium, National Harbor, Maryland January 13-17, 2014.

[3] Wang, Q., Johnson, N., Sprague, M. A. and Jonkman, J. *BeamDyn: A High-Fidelity Wind Turbine Blade Solver in the FAST Modular Framework* 33rd Wind Energy Symposium, AIAA 2015, 5-9 January 2015, Kissimmee, Florida.

[4] Jonkman, J.M., *The new modularization framework for the FAST wind turbine CAEtool*, Proceedings of the 51st AIAA Aerospace Sciences Meeting including the New Horizons Forum and Aerospace Exposition, Grapevine, Texas, January 2013.

[5] Hodges, D. H., *Nonlinear Composite Beam Theory*, AIAA, 2006.

[6] Yu, W. and Blair, M.,*GEBT: A general-purpose nonlinear analysis tool for composite beams*, Composite Structures, Vol. 94, 2012, pp. 2677–2689.

[7] Petersen, J. T., *Kinematically Nonlinear Finite Element Model of a Horizontal Axis Wind Turbine*, Ph.D. Thesis, Risø National Laboratories, DK-4000, Roskilde, Denmark, 1990

[8] Bak, C., Zahle, F., Bitsche, R., Kim, T., Yde, A., Henriksen, L. C., Natarajan, A. and Hansen, M. H. *Description of the DTU 10-MW Reference Wind Turbine*, DTU Wind Energy Report-I-0092, July 2013

[9] Yu, W., Hodges, D. H., Volovoi, V., and Cesnik, C. E. S., *On Timoshenko-Like modeling of initially curved and twisted composite beams*, International Journal of Solids and Structures, Vol. 39, 2002, pp. 5101–5121.

[10] Mayo, J.M., Garcıa-Vallejo, D., and Domınguez, J., *Study of the geometric stiffening effect: comparison of different formulations*, Multibody System Dynamics, Vol.11, 2004, pp.321–341.

[11] Bathe, K. J. and Bolourchi, S., *Large displacement analysis of three-dimensional beam structures*, International Journal for Numerical Methods in Engineering, Vol. 14, 1979, pp. 961–986.

[12] Bauchau, O.A., *Dymore User's Manual*, 2013, http://dymoresolutions.com/dymore40/UsersManual/UsersManual.html.